Size effects in ductile cellular solids. Part I

Onck, P.R.; Andrews, E.W.; Gibson, L.J.

Published in:
International Journal of Mechanical Sciences

DOI:
10.1016/S0020-7403(00)00042-4

Publication date:
2001

PERGAMON International Journal of Mechanical Sciences 43 (2001) 681–699

International Journal of MECHANICAL SCIENCES

www.elsevier.com/locate/ijmecsci

Size effects in ductile cellular solids. Part I: modeling

P.R. Onck[a], E.W. Andrews[b], L.J. Gibson[b,*]

[a]*Micromechanics of Materials, Delft University of Technology, Delft, Netherlands*
[b]*Department of Materials Science and Engineering, Massachusetts Institute of Technology, Room 8-135, 77 Massachusetts Avenue, Cambridge, MA 02139, USA*

Received 20 September 1999; received in revised form 12 May 2000; accepted 15 May 2000

Abstract

In the mechanical testing of metallic foams, an important issue is the effect of the specimen size, relative to the cell size, on the measured properties. Here we analyze size effects for the modulus and strength of regular, hexagonal honeycombs under uniaxial and shear loadings. Size effects for indentation of a honeycomb are evaluated using finite element analysis. Finally, the results for honeycombs are extrapolated to foams. The results are compared with data for metallic foams in the following, companion paper.

Keywords: Cellular-solids; Size effects; Mechanical properties

1. Introduction

The use of metallic foams in lightweight structural sandwich panels or in energy-absorbing devices requires a knowledge of their mechanical properties. Standard test methods are currently being developed (see, for instance, Refs. [1–5]). An important issue is the effect of specimen size on the measured properties. Size effects arise when the macroscopic dimensions of the specimen become of the order of the microstructural length scale of the material: for cellular materials this is the cell size which, for most metallic foams, ranges from about 2–6 mm. The main question addressed here is: how large should a specimen be relative to the cell size in order for the measured response to be indicative of a bulk sample of the material?

Size effects can arise from a change in the constraint of the cell walls at the boundary of a specimen as well as from stress-free cut cell edges at the surface of a specimen. Both effects lead to

* Corresponding author. Tel.: 001-617-253-7107; fax: 001-617-258-6275.
E-mail address: ljgibson@mit.edu (L.J. Gibson).

0020-7403/01/$ - see front matter
PII: S0020-7403(00)00042-4

decreasing moduli as specimen size relative to the cell size decrease. The effect of a change in constraint at the boundaries has been modelled for flexural specimens by assuming that the inner region of the specimen has the modulus of the bulk material while the outer region has a reduced modulus, reflecting the reduced constraint [6]. The model gives a good description of the effect of the ratio of cell size to specimen size on the measured Young's modulus of reticulated vitreous carbon foams. Size effects are also predicted in Cosserat elasticity, which allows for couple stresses. For instance, such size effects have been predicted for two-dimensional gridworks [7], and three-dimensional cubic lattices [8]. Size effects associated with Cosserat elasticity lead to an increase in moduli with decreasing specimen size relative to the cell size. Cosserat effects are difficult to measure but have been observed in rigid polyurethane and polymethacrylimide foams [9,10]. The latter study suggests that surface damage may dominate Cosserat effects in specimens if the damaged layer is as small as 3% of the cell size. For this reason, we do not consider Cosserat effects further in this study.

At low strains open-cell foams deform primarily by elastic bending of the cell edges. At sufficiently high loads, plastic hinges form, giving rise to a stress plateau. In closed-cell foams cell edge bending is accompanied by cell face stretching and yielding, increasing their stiffness and strength above those of open-cell foams. The presence of a variety of defects in the structure of closed-cell metallic foams (for instance, curvature or cracks in the cell walls) reduces the face stretching contribution, giving measured properties only slightly above those expected for open-cell foams. In practice, bending and hinging are the main mechanisms of deformation and failure in both open- and closed-cell metallic foams [11–15].

Idealized, two-dimensional honeycombs have been widely used in understanding the behavior of real three-dimensional foams [16–19]. In this paper we adopt the regular hexagonal structure as our model material, because of its attractive feature of having cell wall bending and hinging as its major deformation mechanisms, similar to its three-dimensional counterpart. We analyze size effects in uniaxial compression (Section 2), simple shear (Section 3), and indentation (Section 4). Results are presented in terms of overall elastic and plastic properties as a function of the ratio of specimen to cell size. Attention is focused on the microstructural origin of the different size effects and its relation to the constraints imposed by the boundary conditions. Finally, suggestions for extending the results to three-dimensional foams are given in the discussion (Section 5). In the companion paper, the analytical results are compared with measurements of the effect of specimen size on the mechanical properties of aluminum foams.

2. Uniaxial loading

Consider an infinitely long, regular hexagonal honeycomb, symmetric with respect to its centerline, loaded in uniaxial compression or tension (see Fig. 1a). For slender cell walls, the deformation is primarily by bending. The cell walls are assumed to be elastic-perfectly plastic and are treated as beams of length L, thickness t, out-of-plane depth, d, moment of inertia I, Young's modulus E_s and yield stress σ_{ys} . The finite width W of the honeycomb is expressed as α times the cell size $D = \sqrt{3}L$; for non-integer values of α, the outer cell walls at the free edges are stress-free. In this section we analyze the Young's modulus and yield stress of the honeycomb as a function of its width.

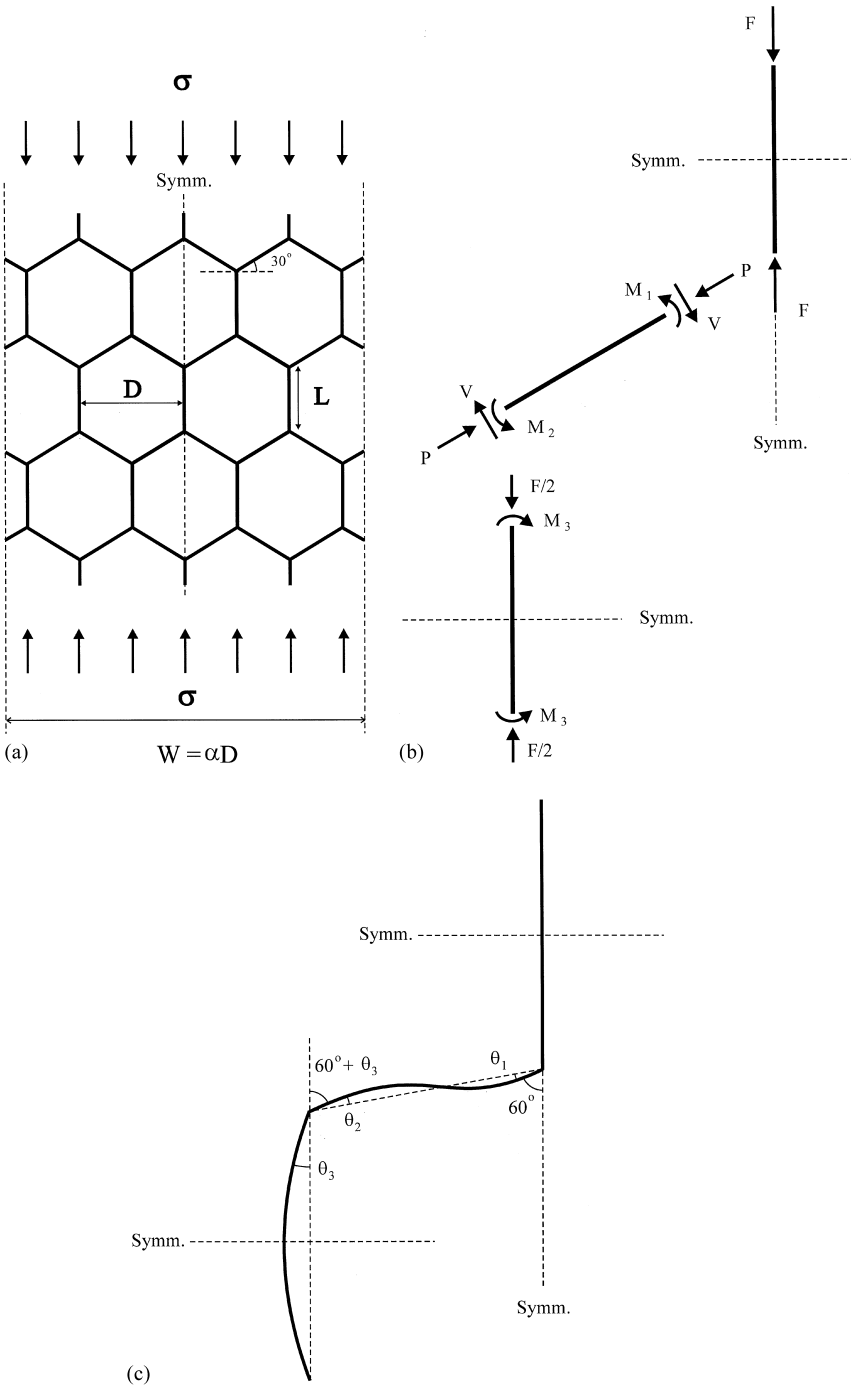

Fig. 1. (a) An infinitely long regular hexagonal honeycomb, loaded uniaxially. The honeycomb is symmetric about its vertical centerline and is of finite width, W. (b) A free body diagram of one quarter of the unit cell for a honeycomb ($W = D$) under uniaxial loading. (c) Deformed configuration of the unit cell of Fig. 1(b).

2.1. Young's modulus

The overall elastic stiffness is calculated from the small strain bending deflection of the cell walls. We first focus on the case. $1 \leqslant \alpha < 2$. Making use of the available symmetries, the problem reduces to that of the free-body diagram of Fig. 1b, where the stress-free outer cell walls are omitted. The force F is related to the applied stress σ by $F = \sigma W d = \sqrt{3}\sigma\alpha L d$. Moment equilibrium in the beams and joints yields

$$-M_1 - M_2 + VL = 0, \tag{1}$$

$$-M_2 + M_3 = 0. \tag{2}$$

Force equilibrium of the left joint in Fig. 1b gives

$$V = \frac{\sqrt{3}F}{4}. \tag{3}$$

To solve for the three moments M_1, M_2, M_3 we use one additional equation of compatibility of deformation (i.e. rotation) of the individual beams. Fig. 1c shows the deformed geometry with the rotations exaggerated for clarity. Since the joints are assumed to be rigid, the beams do not rotate locally relative to each other, leading to the compatibility equation

$$60^\circ + \theta_1 = 60^\circ + \theta_2 + \theta_3. \tag{4}$$

The end-beam rotations are related to the moments by the slope-deflection relations

$$\theta_1 = \frac{M_1 L}{3E_s I} - \frac{M_2 L}{6E_s I},$$

$$\theta_2 = \frac{M_2 L}{3E_s I} - \frac{M_1 L}{6E_s I}, \tag{5}$$

$$\theta_3 = \frac{M_3 L}{2E_s I}$$

leading to

$$M_1 - M_2 - M_3 = 0. \tag{6}$$

Eqs. (1) (2) and (6) enable us to solve for the moments

$$M_1 = \sqrt{3}FL/6$$

and

$$M_2 = M_3 = \sqrt{3}FL/12. \tag{7}$$

Comparing the initial configuration with the deformed configuration (Fig. 1c) yields for the downward displacement δ of the unit-cell (assuming small rotations):

$$\delta = L\cos 60^\circ - L\ \cos(60^\circ + \theta_2 + \theta_3) \approx \frac{\sqrt{3}}{2}L(\theta_2 + \theta_3). \tag{8}$$

Substituting the moments in the slope-deflection relations yields for the rotations $\theta_1 = \theta_3 = \sqrt{3}FL^2/(24E_sI)$ and $\theta_2 = 0$. Comparing this with the solution for the infinitely wide honeycomb, $\theta_1 = \theta_2 = \sqrt{3}FL^2/(48E_sI)$ and $\theta_3 = 0$, Eq. (8) directly shows that the downward displacement δ is twice as large for the finite-sized honeycomb as a result of the large rotation of the outer joint (θ_3). This is related to the released constraint on the outer joint causing the bowing out of the outer cell wall, which is absent in the infinitely wide honeycomb. Using $\varepsilon = 2\delta/(3L)$and $I = dt^3/12$ we find the Young's modulus of the honeycomb

$$E^* = \frac{\sigma}{\varepsilon} = \frac{2E_s}{\sqrt{3}\alpha}\left(\frac{t}{L}\right)^3 \quad \text{for } 1 \leqslant \alpha < 2. \tag{9}$$

Calculations have also been carried out for $2 \leqslant \alpha < 3$ and $3 \leqslant \alpha < 4$, which follow similar lines as above and will not be shown here. Although the calculations are straightforward, they become rather lengthy for large α.

For two larger values of α ($\alpha = 8$ and 16) a finite element analysis was performed using the commercial software package ABAQUS (Hibbitt, Karlson and Sorenson, Pawtucket, RI). Both honeycombs were 17 cells high, a relatively large value, yet necessarily smaller than the infinite height assumed in the analytical solution. The cell walls were assumed to be linear elastic, with $E_s = 70\,\text{GPa}$ and $v = 0.3$ and a thickness-to-length ratio, $t/L = 0.078$. Each cell wall of the honeycomb was modelled using a single beam element; a previous convergence study showed that this was sufficient for convergence [20]. Uniaxial loading was simulated by imposing a uniform displacement in the vertical direction while the sides of the honeycomb were free to move in the horizontal direction. Young's modulus was calculated from the stress (the total force divided by the area of the honeycomb) divided by the strain (the applied displacement divided by the initial height of the honeycomb).

Both the analytical and numerical results are summarized in Table 1 and plotted in Fig. 2, normalized by the reference result for the infinitely wide honeycomb (see Ref. [19].

$$E^* = \frac{4}{\sqrt{3}} E_s\left(\frac{t}{L}\right)^3. \tag{10}$$

Fig. 2 shows that the stiffness is discontinuous at integer values of α. In our analysis, the number of load-carrying vertical beams averaged over the width of the honeycomb increases discretely with α. In a random structure (e.g. a foam) this will clearly not be the case. To account for this in an average manner, a "scatter-band" is constructed by connecting the maxima as well as the minima of the α-intervals (Fig. 2). Clearly, the overall trend is that the stiffness drops considerably for smaller specimens and that it converges to the bulk stiffness for large specimens. The origin of this trend can be traced back to two phenomena: (i) the area fraction of stress-free (non-load-carrying) cell walls increases with decreasing width; (ii) the non-zero rotation of cell-wall joints at the free surface allows for an increased vertical deflection for narrow specimens.

2.2. Plastic collapse

The plastic collapse strength of the honeycomb is calculated using limit load analysis to estimate the upper and lower bounds for the plastic limit state, assuming that the cell walls are perfectly plastic (a good approximation for a wide range of metals and polymers).

Table 1
Normalized compressive Young's modulus and strength

α	$\frac{E^*}{E^*_{bulk}}$	$\frac{\sigma^*_{pl}}{\sigma^*_{bulk}}$
$1 \leqslant \alpha < 2$	$\frac{1}{2\alpha}$	$\frac{1}{\alpha}$
$2 \leqslant \alpha < 3$	$\frac{41}{28\alpha}$	$\frac{2}{\alpha}$
$3 \leqslant \alpha < 4$	$\frac{165}{67\alpha}$	$\frac{3}{\alpha}$
$8 \leqslant \alpha < 9$	$\frac{7.45}{\alpha}$	$\frac{8}{\alpha}$
$16 \leqslant \alpha < 17$	$\frac{15.45}{\alpha}$	$\frac{16}{\alpha}$

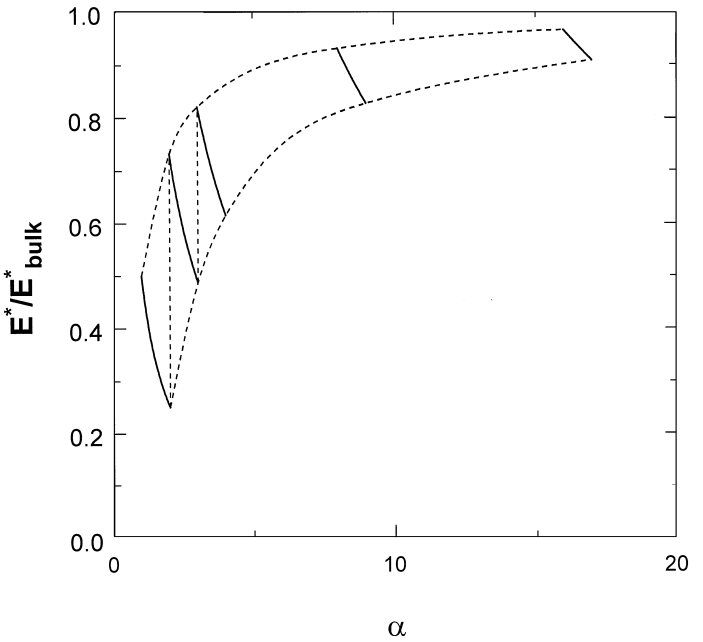

Fig. 2. Young's modulus of a honeycomb of finite width, W, normalized by that of infinite width, plotted against the number of cells across the width, $\alpha = W/D$. The moduli drop between integer values of α since the stiffness of the honeycomb remains constant between one integer value of α and the next while the area of the honeycomb increases. The scatter band is obtained by connecting the maxima as well as the minima of the α-intervals.

An upper bound for the case $1 \leqslant \alpha < 2$ (see Figs. 1a and b) is obtained by considering the kinematically admissible displacement field that develops when plastic hinges form at the end points of the inclined members in Fig. 1b (where the moments M_1 and M_2 act). The upper bound follows from equating the work done by the force F with the plastic work done at the hinges:

$$\frac{\sqrt{3}}{2} FL\phi = 4M_p\phi, \tag{11}$$

where ϕ is the rotation at the hinges and $M_p = \sigma_{ys}\, dt^2/4$ is the plastic moment (neglecting the effect of axial stresses). Substitution of the force $F = \sqrt{3}\sigma\alpha Ld$ and plastic moment M_p yields the upper bound

$$\sigma^*_{up} = \frac{2\sigma_{ys}}{3\alpha}\left(\frac{t}{L}\right)^2. \tag{12}$$

A lower bound can be obtained by analyzing any statically admissible moment distribution, i.e. any distribution of M_1, M_2, M_3 that satisfies Eqs. (1) and (2), the boundary conditions and does not violate yield anywhere. We choose the moment distribution that follows from solving Eqs. (1) and (2) augmented with the condition $M_1 = M_2$, yielding

$$M_1 = M_2 = M_3 = \frac{\sqrt{3}}{8} FL. \tag{13}$$

The lower bound follows from equating the maximum moment with the fully plastic moment M_p, resulting in

$$\sigma^*_{low} = \frac{2\sigma_{ys}}{3\alpha}\left(\frac{t}{L}\right)^2. \tag{14}$$

Since the upper and lower bounds are equal, this must be the exact solution. Repeating the above arguments for larger values of α shows that we can write the results for the plastic collapse stress σ^*_{pl} in the general form

$$\frac{\sigma^*_{pl}}{\sigma^*_{bulk}} = \frac{n}{\alpha}, \quad \text{for } n \leqslant \alpha < n+1,\ n = 1, 2, \ldots \tag{15}$$

with σ^*_{bulk}, the reference value for the infinitely wide honeycomb [19]:

$$\sigma^*_{bulk} = \frac{2\sigma_{ys}}{3}\left(\frac{t}{L}\right)^2. \tag{16}$$

The results are summarized in Table 1 and plotted in Fig. 3. Again, we connect the maxima and minima, showing the average trend of decreasing strength for small specimens and a convergence to the bulk value for large specimens. The decreased strength is directly related to the increased area fraction of stress-free cell walls for small specimens. This causes load shedding to the other cell walls, increasing the net-section-stress and thus lowering the overall yield stress.

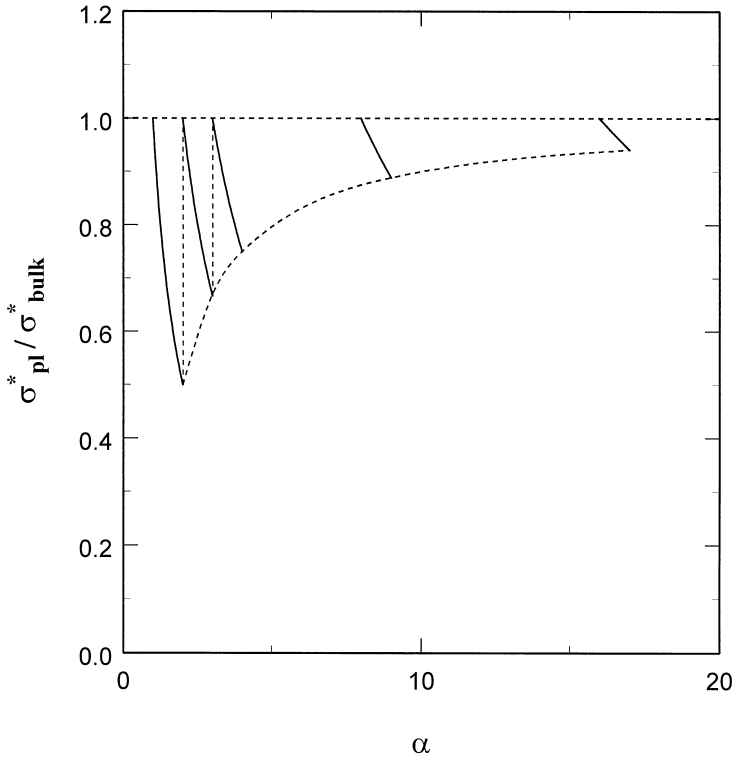

Fig. 3. The uniaxial plastic strength of a honeycomb of finite width, W, normalized by that of infinite width, plotted against the number of cells across the width, $\alpha = W/D$.

3. Shear

We analyze a infinitely wide, regular hexagonal honeycomb loaded in shear by rigid top and bottom plates, as shown in Fig. 4a. The honeycomb has a finite height H with a discrete integer number, n, of cells of dimension, $S = 3L/2$. The cell walls are perfectly bonded to the plates, resulting in clamped boundary conditions. We allow the cell wall lengths at the plates, a and b (see Fig. 4a) to vary according to $a = cL$, $b = (1 - c)L$, with $0 \leqslant c \leqslant 1$, so that $a + b = L$.

3.1. Shear modulus

As in the previous section, we assume that $t \ll L$ so that the honeycomb deforms predominantly by bending, allowing shear and axial deformations of the cell walls to be neglected. We first analyze $H/S = 1$. Incorporating all symmetries yields the periodic unit cell shown in Fig. 4b. The force F is related to the applied shear stress τ according to $F = \sqrt{3}L\tau d$.

We analyze the equilibrium equations in the beams and joints:

$$M_T + M_2^+ - Fa = 0, \tag{17}$$

$$M_2^+ - 2M_2^- = 0, \tag{18}$$

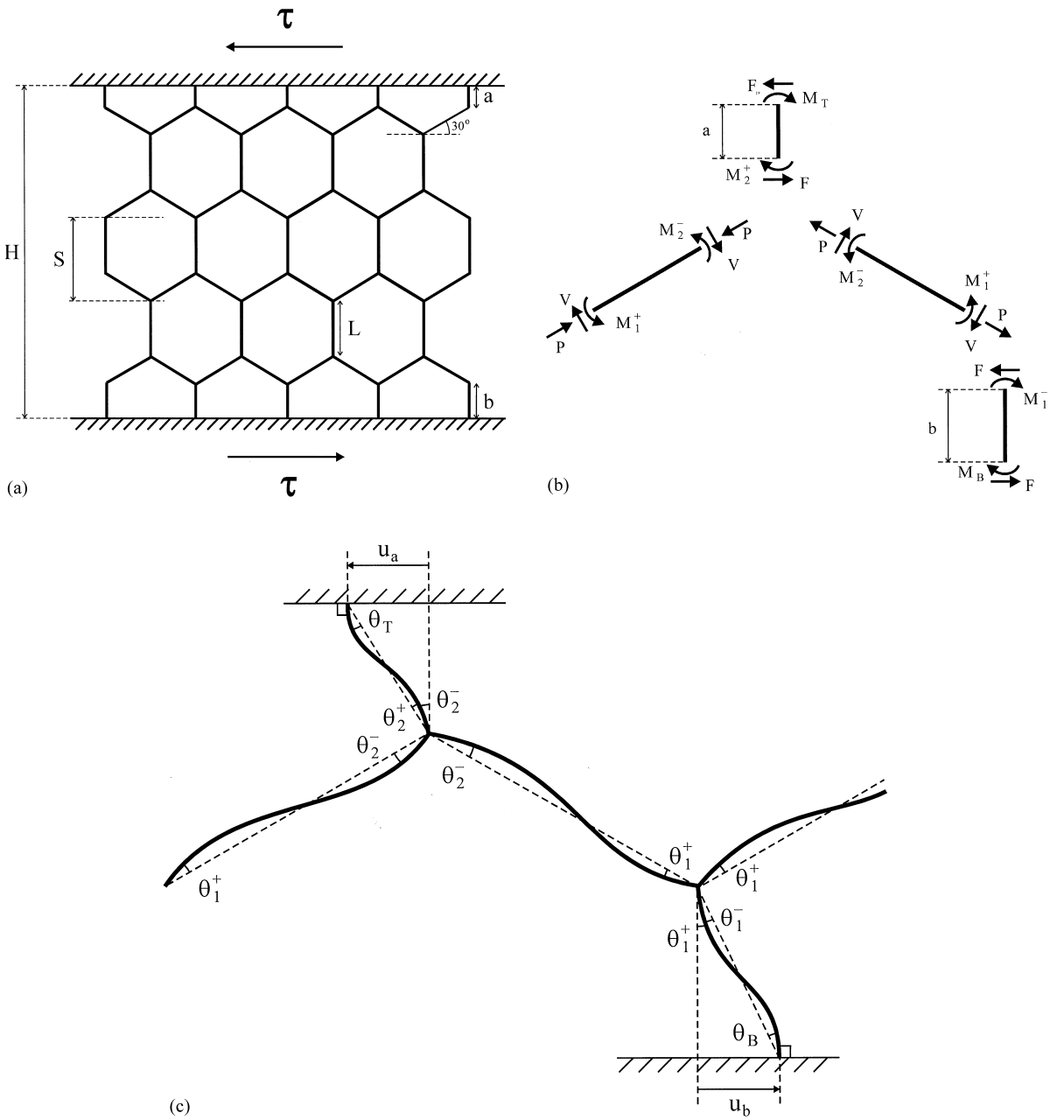

Fig. 4. (a) A regular hexagonal honeycomb of infinite width and of finite height H, loaded in shear by rigid top and bottom plates. (b) A free body diagram of a honeycomb one cell high for shear loading. (c) Deformed configuration of the cell walls shown in Fig. 4(b).

$$-2M_1^+ + M_1^- = 0, \tag{19}$$

$$M_1^- + M_B - Fb = 0, \tag{20}$$

complemented by the compatibility equations for the end-beam rotations

$$\theta_T = \theta_2^- + \theta_2^+, \tag{21}$$

$$\theta_B = \theta_1^- + \theta_1^+, \tag{22}$$

which follow from the deformed configuration shown in Fig. 4c. Substitution of the slope–deflection equations .

$$\theta_B = \frac{M_B b}{3E_s I} - \frac{M_1^- b}{6E_s I}, \quad \theta_1^- = \frac{M_1^- b}{3E_s I} - \frac{M_B b}{6E_s I}, \quad \theta_1^+ = \frac{M_1^+ L}{3E_s I} - \frac{M_2^- L}{6E_s I},$$

$$\theta_2^- = \frac{M_2^- L}{3E_s I} - \frac{M_1^+ L}{6E_s I}, \quad \theta_2^+ = \frac{M_2^+ a}{3E_s I} - \frac{M_T a}{6E_s I}, \quad \theta_T = \frac{M_T a}{3E_s I} - \frac{M_2^+ a}{6E_s I},$$

in Eqs. (8) and (9) yields

$$3a(M_T - M_2^+) + L(M_1^+ - 2M_2^-) = 0, \tag{23}$$

$$3b(M_B - M_1^-) + L(M_2^- - 2M_1^+) = 0. \tag{24}$$

Solving Eqs. (17) –(20), (23) and (24) for the moments and substituting $a = cL$ and $b = (1 - c)L$ yields

$$M_B = -\frac{1}{3}(24c^3 - 54c^2 + 23c + 5)\frac{FL}{A},$$

$$M_1^- = -\frac{2}{3}(12c^3 - 21c^2 + 8c + 2)\frac{FL}{A},$$

$$M_1^+ = \frac{1}{2}M_1^-,$$

$$M_2^- = \frac{1}{3}(12c^3 - 15c^2 + 2c - 1)\frac{FL}{A},$$

$$M_2^+ = 2M_2^-,$$

$$M_T = \frac{1}{3}(24c^3 - 18c^2 - 13c + 2)\frac{FL}{A},$$

where $A = 16c^2 - 16c - 3$.

The shear strain γ is calculated from the deformed geometry (Fig. 4c):

$$\gamma = \frac{u_a + u_b}{\frac{3}{2}L} = \frac{(\theta_2^- + \theta_2^+)a + (\theta_1^- + \theta_1^+)b}{\frac{3}{2}L}. \tag{25}$$

Clearly, the deformation comes from bending of the upper and lower cell walls (associated with θ_2^+ and θ_1^-, respectively) as well as rotation of the joints (associated with θ_2^- and θ_1^+). Substituting

the appropriate rotations and moments, $F = \sqrt{3}L\tau d$ and using $I = dt^3/12$, $a = cL$ and $b = (1-c)L$ gives the shear modulus of the honeycomb one cell high ($H/S = 1$):

$$G^* = \frac{\tau}{\gamma} = \frac{\sqrt{3}E_s A}{8B}\left(\frac{t}{L}\right)^3 \tag{26}$$

with $B = 18c^4 - 36c^3 + 21c^2 - 3c - 1$. Similar calculations have been carried out for $H/S = 2$ and 3 (see Table 2). The results are plotted in Fig. 5 as a function of c, normalized by the reference value for the infinitely wide honeycomb [19]

$$G^*_{bulk} = \frac{E_s}{\sqrt{3}}\left(\frac{t}{L}\right)^3. \tag{27}$$

Fig. 5 shows that for a given H/S, the stiffness is maximum for $c = 0.5$. For $c = 0.5$ the relative stiffening effect is rather high for $H/S = 1$ (4.20) and drops considerably for $H/S = 2$ and 3 (1.50 and 1.29, respectively). For $c = 0$, the stiffening is negligible (1.13, 1.05 and 1.03 for $H/S = 1$, 2 and 3, respectively). Finally, in Fig. 6 the same results are plotted in a different format, using bars to show the range of possible values depending on the value of c.

3.2. Plastic shear strength

Limit load analysis is used to determine upper and lower bounds for the plastic shear strength. We first focus on $H/S = 1$ (Fig. 4b). The upper bound is found from two different kinematically admissible displacement fields. The first is associated with the shearing mechanism for the formation of plastic hinges at the end points of the upper cell walls (of length a, see Fig. 4b). Equating the work done by the force F with the plastic work done at the hinges, yields

$$Fa\phi = 2M_{\mathrm{p}}\phi, \tag{28}$$

where ϕ is the rotation at the hinges and M_p is the fully plastic moment. Substitution of $F = \sqrt{3}L\tau d$, $M_{\mathrm{p}} = \sigma_{\mathrm{ys}}\, dt^2/4$ and $a = cL$ yields the upper bound

$$\tau^{(1)}_{up} = \frac{\sigma_{ys}}{2\sqrt{3}c}\left(\frac{t}{L}\right)^2. \tag{29}$$

Table 2
Normalized shear modulus and strength

$\frac{H}{S}$	$\frac{G}{G_{bulk}}$	$\frac{\tau^*_{\mathrm{pl}}}{\tau^*_{\mathrm{bulk}}}$
1	1.13–4.20	1–2
2	1.05–1.50	1
3	1.03–1.29	1

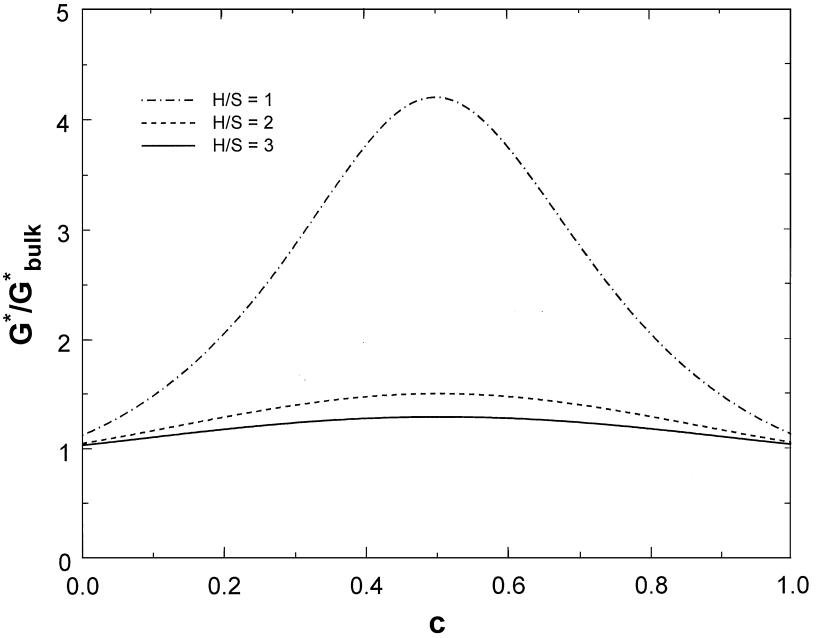

Fig. 5. Shear modulus of a honeycomb of finite height, H, normalized by that of infinite height, plotted against c. $c = a/L$ as shown in Fig. 4a.

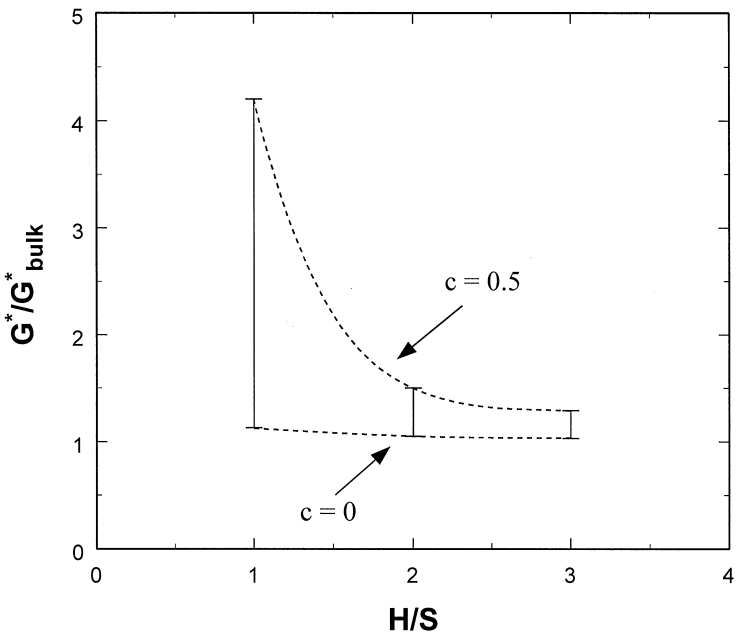

Fig. 6. Shear modulus of a honeycomb of finite height, H, normalized by that of infinite height, plotted against the number of cells along the height, H/S. H is the honeycomb height and S is the cell height, as shown in Fig. 4a.

The second mechanism is associated with plastic hinges at the end points of the lower cell walls (of length b, see Fig. 4b). This yields

$$\tau_{up}^{(2)} = \frac{\sigma_{ys}}{2\sqrt{3}(1-c)}\left(\frac{t}{L}\right)^2. \tag{30}$$

We now consider the minimum upper bound for every value of c, which gives

$$\tau_{\mathrm{up}}\begin{cases}\tau_{up}^{(2)} & \text{for } 0 \leqslant c \leqslant \frac{1}{2},\\ \tau_{up}^{(1)} & \text{for } \frac{1}{2} \leqslant c \leqslant 1.\end{cases} \tag{31}$$

To obtain a lower bound we analyze the statically admissible moment distribution that follows from solving Eqs. (17)–(20) augmented with the equations $M_B = M_1^-$ and $M_T = M_2^+$. This yields

$$M_B = M_1^- = \frac{(1-c)FL}{2},$$

$$M_T = M_2^+ = \frac{cFL}{2},$$

$$M_1^+ = \frac{M_1^-}{2},$$

$$M_2^- = \frac{M_2^+}{2}.$$

The lower bound follows by equating the maximum moment and the fully plastic moment M_p. For $0 \leqslant c \leqslant \frac{1}{2}$, M_B (or M_1^-) is the maximum moment and for $\frac{1}{2} \leqslant c \leqslant 1$ it is M_T (or M_2^+), which yields for the lower bound

$$\tau_{low} = \frac{\sigma_{ys}}{2\sqrt{3}(1-c)}\left(\frac{t}{L}\right)^2 \quad \text{for } 0 \leqslant c \leqslant \tfrac{1}{2}, \tag{32}$$

$$\tau_{low} = \frac{\sigma_{ys}}{2\sqrt{3}c}\left(\frac{t}{L}\right)^2 \quad \text{for } \tfrac{1}{2} \leqslant c \leqslant 1$$

which is identical to the upper bound given in Eq. (31) and therefore must be the exact solution for the plastic limit state. From Eq. (32) we learn that the strengthening effect is at most a factor of 2, which is reached at $c = \frac{1}{2}$ and it vanishes at $c = 0$ (and, equivalently, $c = 1$). Using similar arguments as above for larger (discrete) values of H/S yields solutions that are equal to the plastic shear strength of the infinitely thick specimen [19]

$$\tau_{bulk}^{*} = \frac{\sigma_{ys}}{2\sqrt{3}}\left(\frac{t}{L}\right)^2 \tag{33}$$

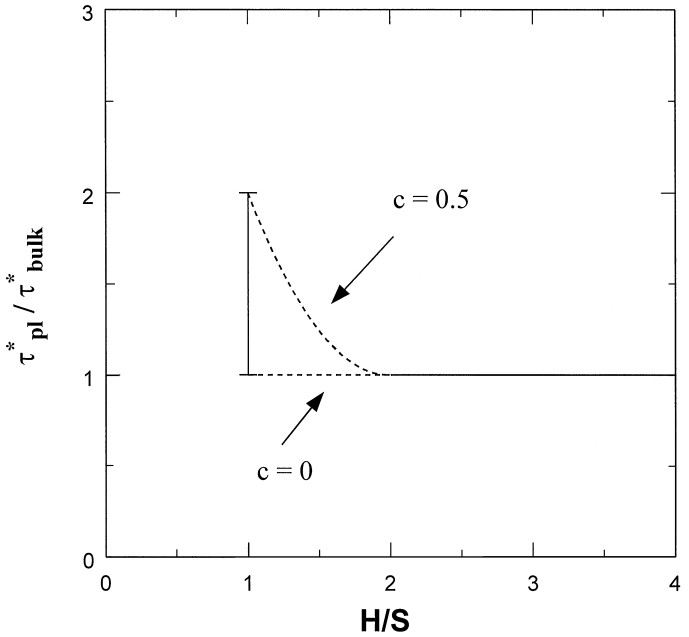

Fig. 7. Shear strength of a honeycomb of finite height, H, normalized by that of infinite height, plotted against the number of cells along the height, H/S.

showing no strengthening effect. The results are summarized in Fig. 7 in a similar format as the shear modulus (Fig. 6). Clearly, the strengthening effect has a rather short range, disappearing for honeycombs two cells high.

4. Indentation

The effect of the size of a rigid indenter on the indentation strength of a regular hexagonal honeycomb of unit depth was modelled using finite element analysis with the commercial software package ABAQUS (Hibbitt, Karlson and Sorenson, Pawtucket, RI). The honeycomb had a width $W = 55\frac{1}{3}S$ and a height $H = 24D$: this size was found to be large enough to eliminate any influence from the boundaries. Three indenter sizes ($w/S = 4$, 8 and 12) were analyzed. The relative density was 0.09 ($t/L = 0.078$). The loading configurations are shown in Fig. 8. The full mesh for one indenter size is shown in Fig. 8(a) while Fig. 8 (b)–(d) show close-up views of each indenter. The solid cell wall material was assumed to be elastic-perfectly plastic with $E_s = 70\,\text{GPa}$, $\nu_s = 0.3$ and $\sigma_{ys} = 300\,\text{MPa}$. Each cell wall was modelled using beam elements. Due to the severe distortion of the cells near the edge of the indenter, four elements per cell wall were required to obtain a convergent solution. The influence of large deformations was included in the simulations. The indenter was displaced uniformly into the honeycomb while the opposite edge of the honeycomb was fixed in the direction of indenter displacement and free to translate in the normal direction.

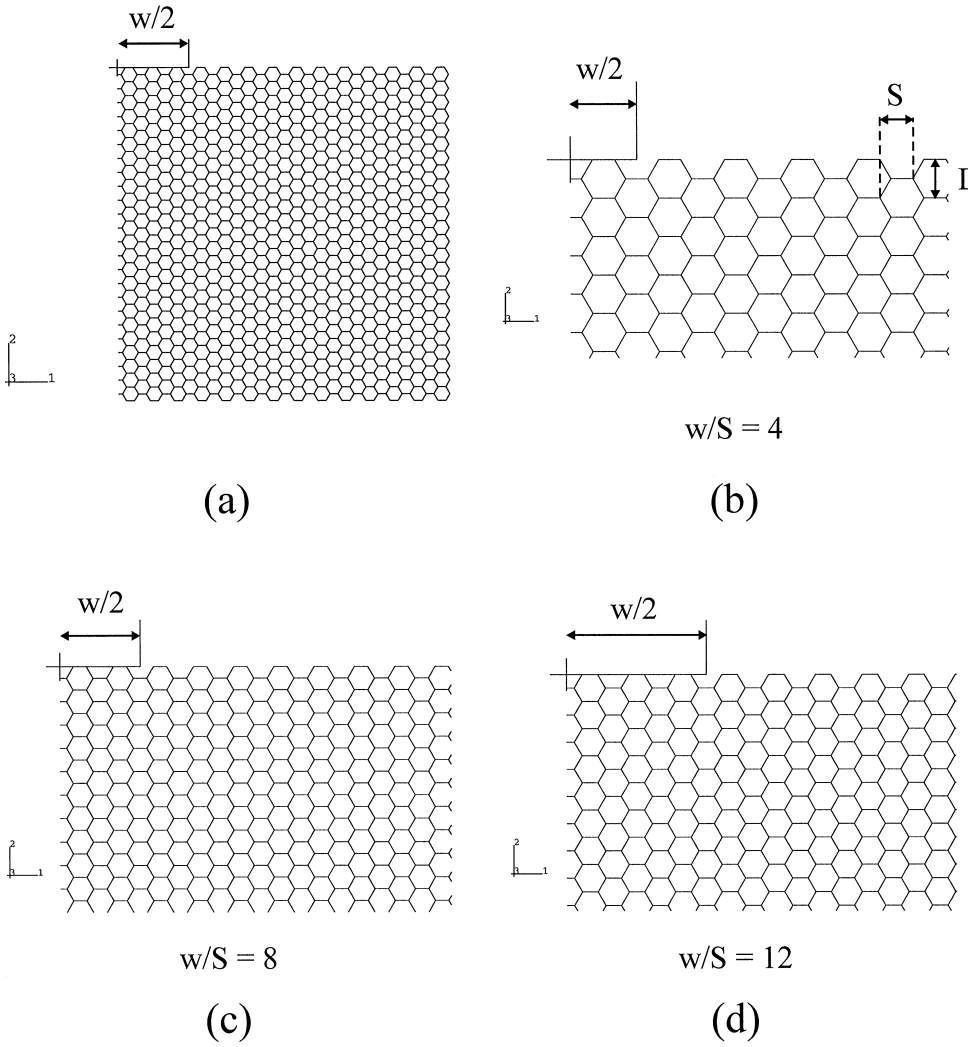

Fig. 8. (a) Full finite element mesh for indentation of honeycombs ($w/S = 12$). (b–d) Finite element mesh for area around the indenter for (b) $w/S = 4$, (c) $w/S = 8$ and (d) $w/S = 12$.

Normalized indentation stress-deformation curves for the three indenter sizes are shown in Fig. 9. The indentation strength was calculated as the total force on the indenter divided by the indenter area. The indentation strength, normalized with respect to the compressive strength, is plotted against the normalized indenter width, w/S, in Fig. 10. As in Figs. 2 and 3, the family of lines showing decreasing indentation stress arises from a constant indentation load with increasing indentater size for indenters which span between cells. Although the indentation stress decreases with increasing punch diameter, the dependence is weak.

The decrease in the indentation strength as the ratio of the indenter size to the cell size increases can be understood as follows. The total load on the indenter (of width w and depth d) is the sum of

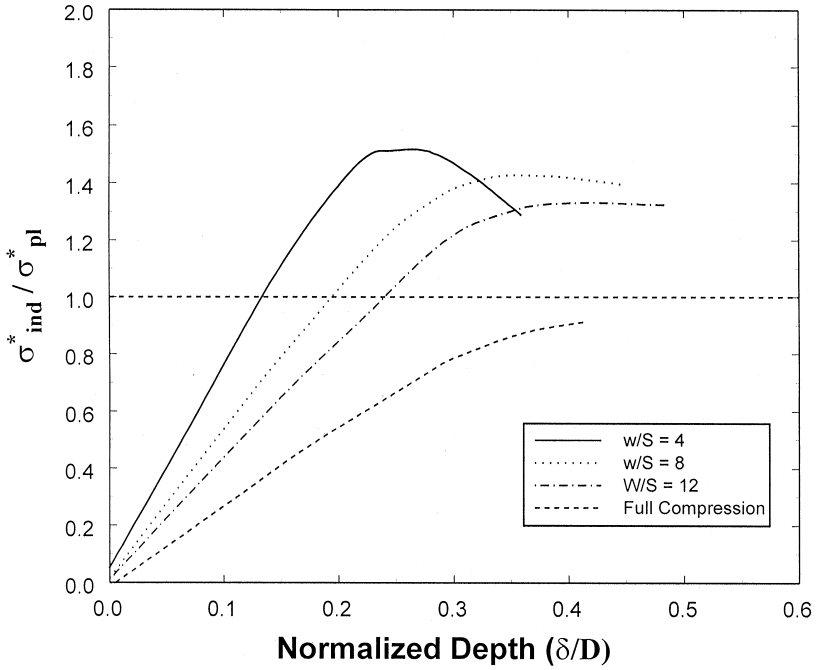

Fig. 9. Normalized indentation stress plotted against normalized deflection for indentation of a honeycomb. A uniaxial stresss–strain curve for the honeycomb is included for comparison.

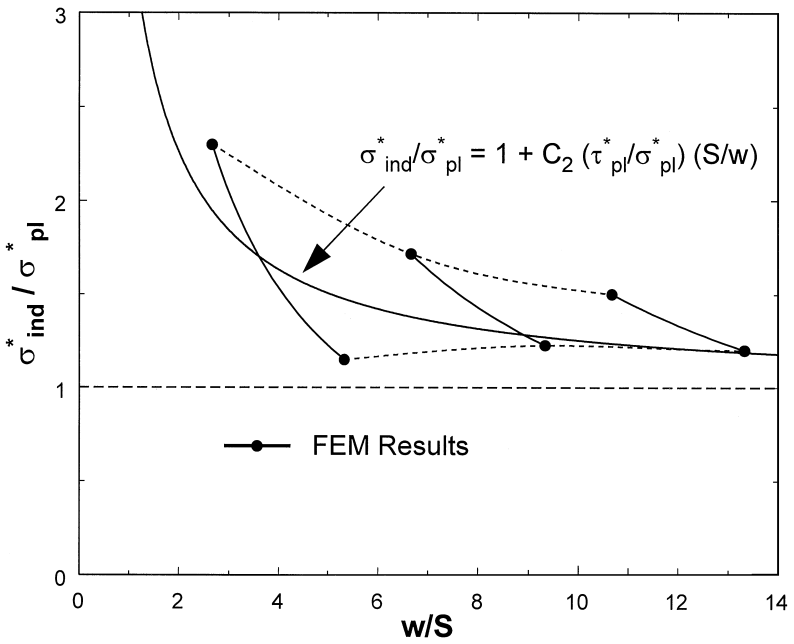

Fig. 10. Normalized indentation strength plotted against the ratio of indenter width to the cell size, w/S.

that required to crush the honeycomb beneath the indenter and that required to fully yield (and then tear) the cell walls at the perimeter of the indenter:

$$P_{total} = \sigma^*_{pl} wd + C_1 \tau^*_{pl}(2D)d$$

or

$$\frac{\sigma_{ind}}{\sigma^*_{pl}} = 1 + C_2 \frac{\tau^*_{pl}}{\sigma^*_{pl}} \frac{S}{w}. \tag{34}$$

This equation is also plotted in Fig. 10: it gives an approximation of the finite element results but is not an exact description of them. A similar expression for foams (Eq. (37)) does give a good description of the experimental indentation results, described in the next paper, suggesting that the details of the indentation process may differ for the foam and the honeycomb. As an estimate, we have used the finite element results to obtain a value for $C_2 = 7.23$, giving $C_1 = C_2/2(D/S) = 3.14$. This suggests that shearing at the edge of the indenter occurs over a depth of about three cells. Note also that the ratio of the shear strength to the compressive strength of a regular hexagonal honeycomb is 0.433. For large indenter sizes (relative to the cell size) the indentation strength approaches the uniaxial compressive strength of the honeycomb.

5. Discussion

The Young's modulus of a regular hexagonal honeycomb increases up to a plateau value, representative of the bulk material, for integer values of the ratio, α, of the honeycomb width, W, to the cell size, D. For narrow specimens, the non-zero rotation of the joints at the free surface allows for increased deflection, decreasing the modulus below that of the bulk. For non-integer values of α, the inclined cell edges at the free surface are cut so that they carry no load. As α increases from one integer value to the next, the area fraction of non-load-carrying cell walls increases, reducing the modulus.

In a foam, we expect that the cell edges and faces near the free surface are, like those in the honeycomb, less constrained than those in the bulk. We also expect that in an open-cell foam, as in the honeycomb, there are stress-free cut edges at the surface layer. We model both effects by considering a square prismatic specimen of foam of width L and cell size d^* ($L = \alpha d^*$), following the method of Brezny and Green [6]. Well away from the outer surface, in the core of the material, the material has a Young's modulus E_{bulk}. There is a boundary layer around this core of lower stiffness, reflecting the reduced constraint near the surface: we model this boundary as a layer of thickness nd^* with Young's modulus mE_{bulk} (with $0 \leqslant m \leqslant 1$). At the corners of the boundary layer, the Young's modulus is even lower; we take it to be $m^2 E_{bulk}$. In an open cell foam, the boundary layer is, in turn, surrounded by a surface layer of thickness pd^* with cut cell edges of zero stiffness. The effective Young's modulus of the material is then

$$\frac{E^*}{E^*_{bulk}} = \left(1 - 2n\frac{d^*}{L} - 2p\frac{d^*}{L}\right)^2 + 4nm\left(\frac{d^*}{L}\right)\left[1 - 2n\left(\frac{d^*}{L}\right) - 2p\left(\frac{d^*}{L}\right)\right] + 4n^2m^2\left(\frac{d^*}{L}\right)^2, \tag{35}$$

The flat faces of most closed-cell foams provide some support to the cut edges. In practice, the closed-cell aluminum foam tested in the companion study has been found to behave mechanically like an open-cell foam due to microstructural imperfections such as cell wall curvature [21]. For the aluminum foam tested as part of this study, we assume that the faces do not stiffen the cut cell edges at the surface appreciably.

On average, the plastic collapse strength of a honeycomb increases with increasing α up to a plateau value representative of the bulk material. The reduced strength for small specimens is caused by the presence of a layer of cell walls at the free edge that does not carry load; on average, this layer is one-fourth of a cell size thick. The analysis can be extended to foams by considering a square prism of foam of width αd^* (d^* is the cell size), with a layer of $d^*/4$ thick at the surface that does not carry load. Equating the applied force at plastic collapse, $\sigma_{pl} d^{*2} \alpha^2$, with the force in the foam, $\sigma_{bulk} d^{*2} (\alpha - \frac{1}{2})^2$ yields

$$\frac{\sigma_{pl}}{\sigma_{bulk}} = \frac{(\alpha - \frac{1}{2})^2}{\alpha^2}. \tag{36}$$

This relation directly carries over the size-effect found in honeycombs to foams. It can be used as an approximation for the effect of the ratio of specimen size to cell size on the uniaxial compression strength of foams.

The calculations of the shear stiffness and strength (see Section 3) were performed for an idealized, regular, hexagonal honeycomb. Based on dimensional arguments, they do not need extrapolation to three dimensions as the compression results did, as stress or strain gradients in the third (out-of-plane) direction do not develop when the foam is thick enough. Consequently, no size-effects are present in this direction and the results for the two-dimensional honeycomb can be used as an approximation for the size effect in shear in three-dimensional foams.

Dimensional arguments suggest that for a foam loaded by a circular indenter, the indentation strength is related to the cell size d^* and the indenter radius R by

$$\frac{\sigma^*_{ind}}{\sigma^*_{p1}} = 1 + C_1' \frac{\tau^*_{p1}}{\sigma^*_{p1}} \frac{d^*}{R}. \tag{37}$$

The results of the models are compared with data for the uniaxial modulus and strength, and the shear and indentation strengths of aluminum foams in the following companion paper.

Acknowledgements

We would like to acknowledge the assistance of Prof. J.W. Hutchinson, of the Division of Engineering and Applied Sciences at Harvard University. The research of Dr. P. Onck was made possible by a fellowship of the Royal Netherlands Academy of Arts and Sciences. Financial support of this project was provided by the Advance Research Project Agency through the Multi-University Research Initiative (MURI) under Office of Naval Research Contract No. N-00014-1-96–1028.

References

[1] Gradinger R, Simancik F, Degischer HP. Determination of mechanical properties of foamed metals. International Conference Welding Technology, Materials and Materials Testing, Fracture Mechanics and Quality Management, Vienna University of Technology, 1997.

[2] Sugimura Y, Meyer J, He MY, Bart-Smith H, Grenestedt J, Evans AG. On the mechanical performance of closed cell foams. Acta Materlia 1997;45:5245–59.

[3] Simone AE, Gibson LJ. Aluminum foams produced by liquid state processes. Acta Materlia 1998;46:3109–23.

[4] Von hagen H, Bleck W. Compressive, tensile and shear testing of melt-foamed aluminum. Symposium R: Porous and Cellular Materials for Structural Applications, Materials Research Society Spring Meeting 1998 San Francisco, 1998.

[5] Ashby MF, Evans AG, Fleck NA, Gibson LJ, Hutchinson JW, Wadley HNG. Metal foams: a design guide. London: Butterworths, 2000.

[6] Brezny R, Green DJ. Characterization of edge effects in cellular materials. Journal of Material Science 1990;25:4571–8.

[7] Askar A, Cakmak AS. A structural model of a micropolar continuum. International Journal of Engineering Science 1968;6:583–9.

[8] Adomeit G. Determination of elastic constants of a structured material. In: Kroner E, editor. Mechanics of Generalized Continua. IUTAM Symposium, Freudenstadt. Stuttgart, Springer 1967.

[9] Lakes RS. Experimental microelasticity of 2 porous solids. International Journal of Solids and Structures 1986; 22:55–63.

[10] Anderson WB, Lakes RS. Size effects due to cosserat elasticity and surface damage in closed-cell polymethacrylimide foam. Journal of Material Science 1994;29:6413–19.

[11] Simone AE, Gibson LJ. The effects of cell face curvature and corrugations on the stiffness and strength of metallic foams. Acta Materlia 1998;46:3929–35.

[12] Grenestedt JL. Influence of wavy imperfections in cell walls on elastic stiffness of cellular solids. Journal of Mechanics and Physics of Solids 1998;46:29–50.

[13] Andrews EW, Sanders W, Gibson LJ. Compressive and tensile behavior of aluminum foams. Materials Science and Engineering A 1999a;270:113–24.

[14] Bart-Smith H, Bastawros A-F, Wadley HNG. Compressive deformation and yielding mechanisms in cellular Al alloys determined using X-ray tomography and surface strain mapping. Acta Materlia 1998;46:3583.

[15] Chen C, Lu TJ, Fleck NA. Effect of imperfections on the yielding of two-dimensional foams. Journal of Mechanics and Physics of Solids 1999;47:2235–72.

[16] Gibson LJ, Ashby MF, Schajer GS, Robertson CI. The mechanics of two-dimensional cellular materials. London, Proceedings of the Royal Society 1982;A382:25–42.

[17] Warren WE, Kraynik AM. Foam mechanics: the linear elastic response of two-dimensional spatially periodic cellular materials. Mechanics of Materials 1987;6:27–37.

[18] Papka SD, Kyriakides S. In-plane compressive response and crushing of honeycomb. Journal Mechanics and Physics of Solids 1994;42:1499–532.

[19] Gibson LJ, Ashby MF. Cellular solids: structures and properties, 2nd ed. Cambridge: Cambridge University Press, 1997.

[20] Silva MJ, Gibson LJ, Hayes WC. The effects of non-periodic microstructures on the elastic properties of two-dimensional cellular solids. International Journal of Mechanical Sciences 1995;37:1161–77.

[21] Andrews EW, Gioux G, Onck PR, Gibson LJ. Size effects in metallic foams Part II: experimental results. International Journal of Mechanical Sciences 2001;43:701–13.